

# Numerical Study of the Mechanical Behavior and Fatigue in a Weld Bead by Friction Stir for a 6082-T6 Aluminum Alloy

Youb Kambouz<sup>1\*</sup>, Mohamed Benguediab<sup>1</sup>, Benattou Bouchouicha<sup>1</sup>, Mohamed Mazari<sup>1</sup>

Received 19 March 2016; accepted after revision 23 November 2016

## Abstract

*The process of friction stir welding is a significant advance in the field of research on the Friction welding technique known for several decades. This assembly technique has obvious originality since welding is performed in the solid state, which can help eliminate birth defects related to solidification phase compared to conventional welding.*

*The numerical modeling of this type of process is complex, not only in terms of the variety of physical phenomena which must be considered, but also because of the experimental procedure that must be followed in order to verify and validate numerical predictions. In this work, a finite element model is proposed in order to simulate the crack propagation under monotonic loading in different areas of the weld seam of a specimen CT-50 aluminum alloy 6082-T6.*

*Microhardness tests were performed to characterize the Vickers hardness profile in the vicinity of the weld area. Friction stir welding process leads to a decrease of the static mechanical properties relatively to base material. Detailed examination revealed a hardness decrease in the thermo mechanically affected zone and the nugget zone average hardness was found to be significantly lower than the base alloy hardness. Welded specimens show significantly lower lives than base material.*

## Keywords

*Friction Stir Welding, aluminium alloy, microstructure, mechanical properties, fatigue*

## 1 Introduction

Considered as the most significant development in metal joining in the last decade, the Friction Stir Welding (FSW) is a joining process with good energy efficiency that is also environmentally friendly and versatile. Significant research has been conducted in various fields since the invention of this technique in 1991, [1]. Generally, FSW specimens have higher resistance than specimens welded using the Metal Inert Gas (MIG) and Tungsten Inert Gas (TIG) processes. [2] and [3], compared fatigue results of friction stir welds with data obtained for conventional arc-welding methods, namely, MIG-pulse and TIG processes in aluminum alloy (T6 and T4 conditions). [4, 5] also compared the fatigue behaviour of joints performed by the traditional MIG welding process and by the FSW process, observing that FSW and MIG welded specimens had lower yield and ultimate stresses than the base material. In general, a higher lifetime for the friction stir welds in comparison with other welds was also observed by [6]. It has also been observed that FSW leads to a decline of the mechanical properties of weld bead in comparison to the base metal [7]. Furthermore, an important hardness decrease in the Thermomechanically Affected Zone (TMAZ) and a nugget zone average hardness was recorded.

Due to severely thermal and mechanical deformation in the weld zone during FSW, this zone generally possesses various microstructural features and various mechanical properties [8] and [9]. The crack propagation in the weld bead (FSW and classic) is known to be concerned by residual stress and/or hardness around the welded zone [10] and [11]. [12] Conducted hardness tests on micro-specimen.

The limit of elasticity, tensile strength and Young's modulus (E) of the aluminum alloy (6082-T6) were measured using tensile tests on welded and non-welded specimens. Modeling the tensile behavior of welded FSW for an aluminum alloy joint showed that the weak area is the HAZ, [13]. Welding parameters also affect the mechanical properties of the weld and its resistance is related to the speed of rotation of the welding tool [14] and [15]. [16] studied the effect of rotational speed, welding speed, axial force, shoulder diameter, pin diameter and tool

<sup>1</sup> Laboratory of Materials and Reactive Systems LMSR, University Djillali, Liabes, Sidi Bel-Abbes, Algeria

\*Corresponding author, e-mail: [y\\_kambouz@yahoo.fr](mailto:y_kambouz@yahoo.fr)

hardness on the strength properties of AA7075-T6 aluminium alloy. It is therefore advisable to choose the best parameters speed, welding speed and good fixation of the parts [17].

## 2 Presentation of the material

The material used is an aluminum alloy 6000 series subjected to T6 treatment, which will help the investigation of the various phenomena that occur during welding with involving the precipitation phenomenon.

This aluminium alloy is a high strength Al–Mg–Si alloy that contains manganese to increase ductility and toughness. The T6 condition is obtained through artificial ageing at a temperature of approximately 180°C [2].

The alloy chemical composition and mechanical properties are shown in Tables 1 and 2, respectively.

**Table 1** Chemical composition of AA 6082-T6 aluminum alloy (wt %).

Si	Mg	Mn	Fr	Cr	Cu	Zn	Ti	Al
1.3	1.2	1.0	0.5	0.25	0.1	0.2	0.1	98.3

**Table 2** Tensile properties for base materials [18].

Material	E[MPa]	$\sigma_e$ [MPa]	$\sigma_{max}$ [MPa]	$\epsilon$ [%]	n	K[MPa.m <sup>1/2</sup> ]
Al6082T6	69000	260	366	13.3	0.10	22

### 2.1 Experimental procedure

The friction stir welding was performed with the following conditions:

- The machine is a universal milling machine
- A tool with a diameter of 5 mm and that of the shoulder equal to 12 mm.
- The rotational speed equal to 1400 rev / min
- The advance speed equal to 80 mm / min.
- Parts made have suffered as microhardness testing, on a device HMV 2000.

Tensile and fatigue tests were simulated using ABAQUS.

### 2.2 Hardness profile and Microstructure of the 6082-T6 FSW joint

The optimization of the weld process requires the mechanical characterization of the weld bead. The most commonly used practice is the measurement of microhardness which gives a first evaluation of the mechanical properties in different areas of the weld, in order to obtain a profile across it and to establish the weld zones. The cross-section thus provides a profile of microhardness [19]. The Vickers hardness profiles for all areas (BM, HAZ, TMAZ and nugget) are presented in Fig. 1. A hardness decrease occurs when approaching the TMAZ. The average hardness of the nugget zone (NZ) was found to be significantly lower than the hardness of the base alloy. There is a zone

outside the nugget (transition between TMAZ and HAZ) which has the lower hardness value. In [9] and [20], it is suggested that the variation of the microhardness values in the welded area and parent material is due to the difference between the microstructures of the base alloy and weld zone.

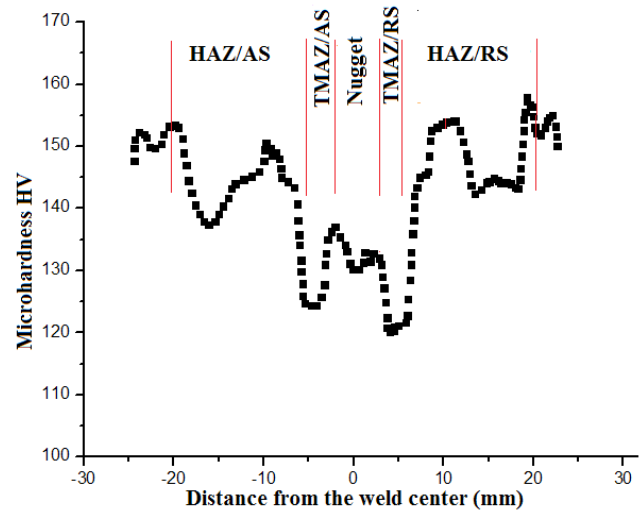


**Fig. 1** Hardness profile

Pictures of the microstructure of the different areas of the 6082-T6 alloy aluminum can be found in [21].

An recrystallization was observed in nugget. By moving towards the BM, no recrystallization was observed in TMAZ and in HAZ.

Optical micrographs of the thin friction stir welded joint are illustrated in Fig. 2. The weld exhibits distinct regions as shown in on these figures.

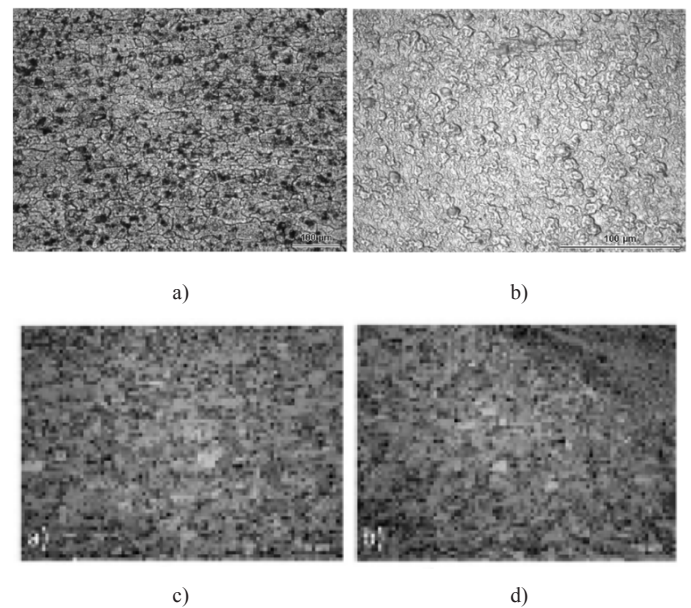


**Fig. 2** The Base Material (or parent material), HAZ, TMAZ and Nugget for the 6082-T6 [21], a) Grains of base material, b) Nugget with its fine recrystallized grains, c) Grains of TMAZ, d) Grains of HAZ

### 2.3 Numerical protocol and mechanical properties of the material

The tensile test is modeled and simulated in the calculation software Abaqus FEA. This step requires the setting of many sizes and choices in the model which are explained in this study.

A displacement along the axis “y” is imposed. A fault is inserted to initiate and locate the break.

The numerical method was performed using standard rectangular tension test specimens [22], Fig. 3.

The geometry of the specimen is created under the 2D software. Geometry and boundary conditions are defined in Fig. 4.

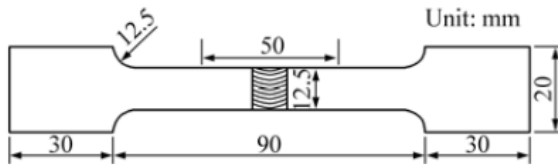


Fig. 3 Tensile Specimen

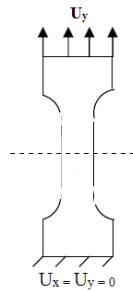


Fig. 4 Geometry and boundary conditions in the simulation of a tensile test.

The calculations are made in explicit because the removal of the elements is managed directly by Abaqus. The explicit approach depends on the size of the mesh.

By refining the mesh, the calculation time increases. It is therefore preferable to use a coarse mesh. However, it is also necessary to refine the crack tip mesh to visualize phenomena such as plasticity.

FSW joints in 6082-T6 aluminium alloys of 6 mm in thickness were subjected to a number of tensile tests. The aim of this work is to gain some understanding on mechanical properties and on the effect of plastic deformation on the microstructure of thin aluminium alloy FSW joints.

Figure 5 shows a broken test specimen under Abaqus software.

Table 3 presents the tensile properties for friction stir welded specimens and base material.

The test results from the 6082-T6 welds are lower than the parent material due to thermal softening.

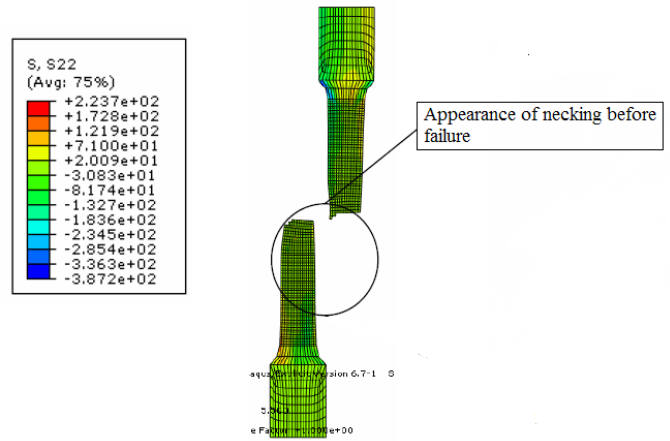


Fig. 5 2D simulation of a tensile test.  $S_{22}$  constraints after the failure

Results of tensile tests simulation on unwelded and welded samples, performed in this paper, are here mentioned in Table 3, these tests showed a remarkable reduction of both tensile strength (from ~320 MPa down to 200 MPa) and elongation (from ~ 16% down to ~ 7%) as compared with nominal.

The softest points of the joints correspond to the failure locations in tensile tests.

In practice for each set of welding parameters, local tensile strength and local ductility vary widely. In turn, variations in these local conditions result in different bulk tensile strengths and bulk ductility [17]. The lowest Tensile Strength found for welds in FSW for 6082-T6 was 64% of the base metal strength. This variety suggests that parameters can be tailored in order to impart desired weld characteristics.

Three tests were performed for each area by changing the mesh to be closer to experimental test.

### 3 Modeling of the specimen CT-50

The calculations are made in two dimensions to meet the time constraint. Similarly, only half CT50 specimen is modeled.

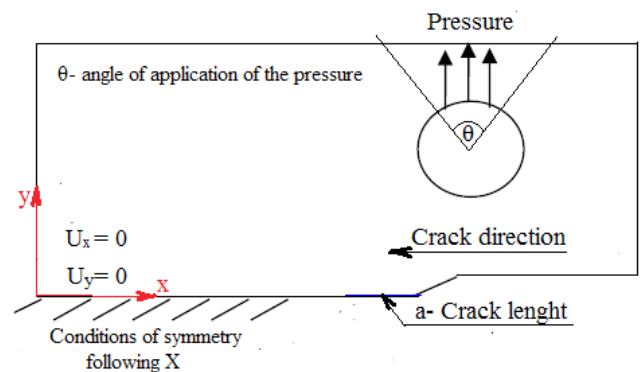


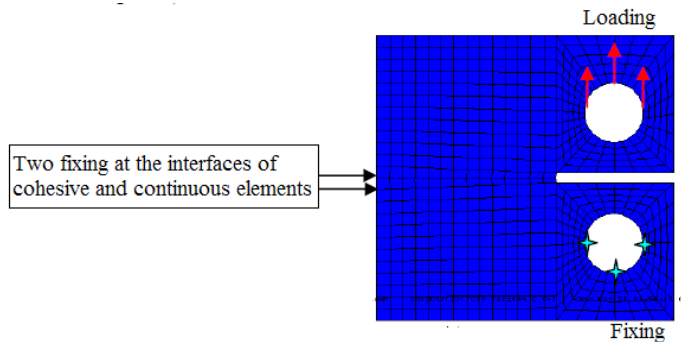
Fig. 6 Modeling of the specimen CT-50 and boundary conditions.

**Table 3** Results of tensile tests on unwelded and welded samples

N°	Sample	Tensile strength [MPa]	Zones of rupture	Elongation %	Hardness, Hv
1	Base material	322.6	BM	16.8	110
2	Base material	323.4	BM	15.2	
3	Base material	322.7	BM	16.5	
-	Average	322.9	BM	16.2	
1	As welded	286	Nugget	10.8	78 to 84
2	As welded	279	Nugget	10.4	-
3	As welded	218	HAZ/TMAZ	7.5	-
4	As welded	221	HAZ/TMAZ	8.6	-
5	As welded	230	HAZ/TMAZ	8.4	-
6	As welded	225	HAZ/TMAZ	8.7	75 to 85
7	As welded	211	HAZ	7.4	65 to 109
8	As welded	207	HAZ	7.0	-
9	As welded	213	HAZ	7.3	-
10	As welded	209	HAZ	7.2	65 to 109

**Table 4** Material parameters entered in Abaqus

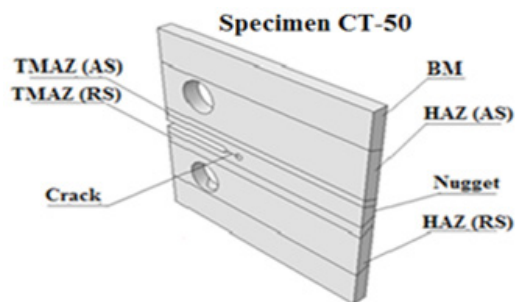
	6082-T6	6082-T6 (FSW)
$E$ [MPa]	68000	51200
$R_p$ [MPa]	265	135.8
$C$ [MPa]	1100	1100
$s$	0.93	0.93
$S$ [MPa]	2	2

**Fig. 8** Cohesive elements and boundary conditions.

### 3.1 Modeling of the cracked part

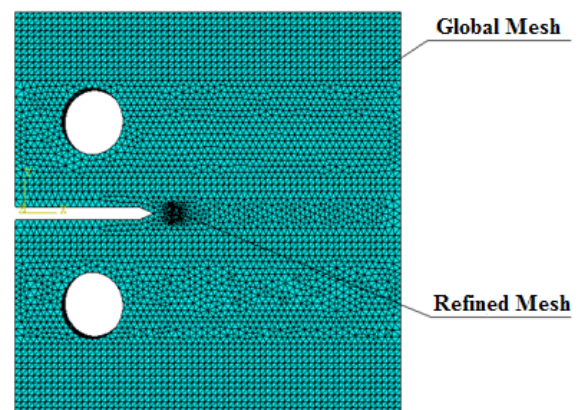
The modeled weld is divided into several zones, as shown in Fig. 7, and a different mechanical behavior is assigned for each.

In the model considered in this paper, the areas are fully supportive of each other, movement is continuous and normal stress is transmitted. This model allows the obtainment of a mapping of local deformations through a welded joint (Fig. 8). The part is a CT-50 specimen, the cracking plane is considered normal to the loading axis and the crack front is considered straight.

**Fig. 7** Representation of welding areas.

### 3.2 Mesh of the cracked part and Boundary conditions

The numerical analysis of the mechanical fields of a cracked part is strongly linked to the meshing quality of this part, particularly the vicinity of the crack tip. It is therefore important to manage the mesh to the crack tip Fig. 9.

**Fig. 9** Mesh of the specimen.



The master surface is coarsely meshed and corresponds to the continuous elements.

The slave surface is finely meshed and corresponds to the cohesive elements.

## 4 Numerical results

### 4.1 Numerical modeling

The simulation is performed by explicit. A specimen test CT-50 is modeled in computing software by finite element. The geometry of the specimen and the modeled conditions limits applied are shown in Figs. 7 and 8.

The mesh is refined only at the crack tip for limit the duration of the calculation. In this area, the mesh size is between  $10^{-3}$  and  $10^{-2}$  mm.

Loading  $F$  obeys a sinusoidal law inserted under the software as periodic amplitude:

$$F = F_{sta} + F_{amp} \sin(2\pi ft) \quad (1)$$

The values of  $F_{stat}$  and  $F_{amp}$  are related to  $R = 0.1$ , charge ratio.

Upload is modeled by a pressure  $P$ , defined on the upper surface of the hole of the CT test piece, as shown in Fig. 8.

It is introduced in two stages during the calculation. In the first “Step” static  $F_{sta}$  is applied. Then the cyclic loading is superimposed in a second “Step”.

This division is necessary because the calculation converges difficult if the loads are applied simultaneously. Similarly, the frequency should not be too high because otherwise the explicit calculation diverges or the energy criterion,  $E_{kinetic} \ll E_{internal}$ , ensuring the validity of the results is not checked. The choice of timing parameters take into account the convergence calculations, the energy criterion, and the need for acceptable calculation times.

### 4.2 Visualization of the crack propagation

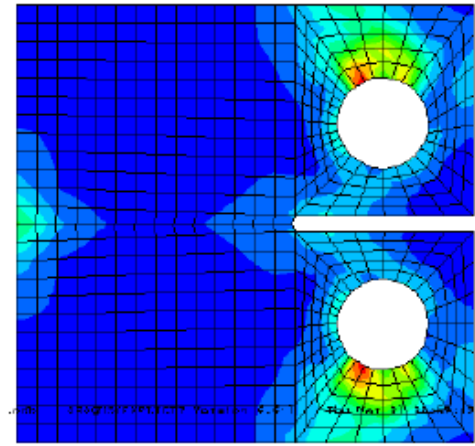
More than a failure criterion may be associated with calculation. A criterion consists of two stages, the initiation and propagation:

- Initiation:

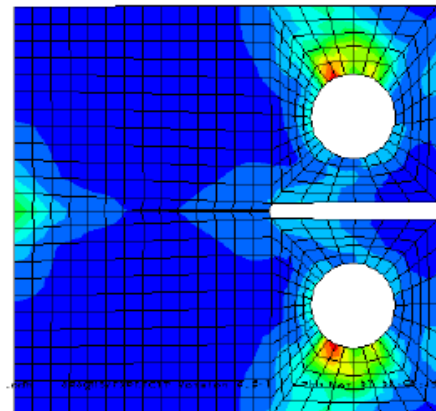
This step corresponds to the beginning of the damage. It starts when the stresses and deformations satisfy an initiation test. This phase is in no way associated with a law of propagation and does not model the damage process.

- Evolution of damage:

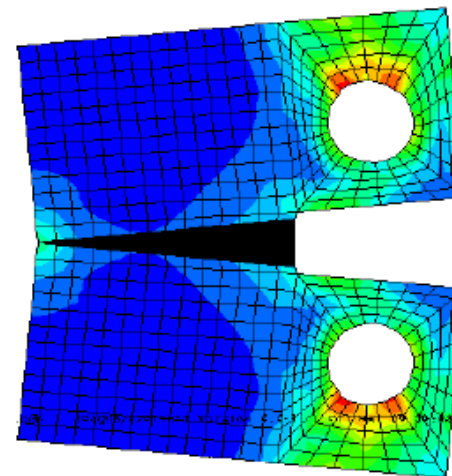
A damage evolution law describes the percentage of degradation of the material in the thickness when the initiation criterion is reached. A variable  $D$ , characterizing damage and actual nominal stresses is introduced:



The load is applied gradually. The crack does not spread.



The crack appears. Moving jump has reached the critical value.



Specimen is fully open.

Fig. 10 Visualization of the crack propagation

### 4.3 Numerical determination of the curve

#### $da/dN = f(\Delta K)$

The first objective is to compare the curves of Wohler for the different areas of welding FSW.

The Wohler curves reach clear differences between 6082-T6 (BM) and Nugget, TMAZ and HAZ. The comparison of curves (SN) characteristics of welded joints by FSW and those of the base material shows that the fatigue strength of welded joints is significantly smaller than the base material except for a few points in the areas of medium lives (Fig. 11).

Fatigue results obtained in this work are close with data obtained by other authors [23] for this welding process FSW.

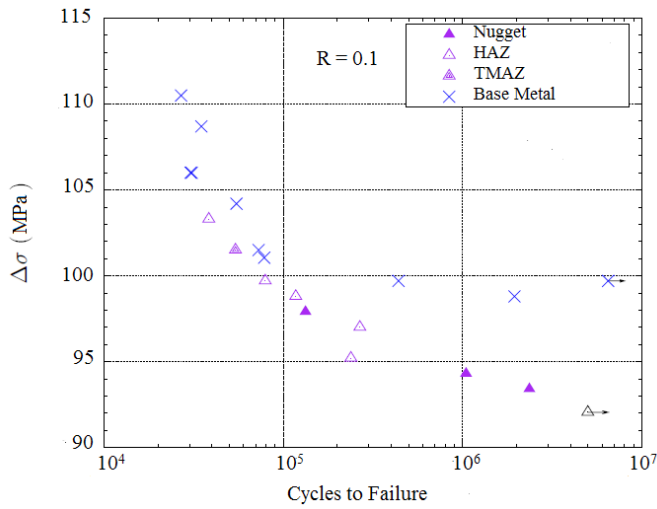


Fig. 11 Fatigue endurance curves for the joints welded and base metal.

The second objective is not to simulate the crack propagation test for strong  $\Delta K$ , but to digitally generate the  $da/dN$  curve according to  $\Delta K$ . Therefore, we opted for a stepwise approach. This method consists of performing several simulations at different values of  $\Delta K$  for determining the speed of propagation of the  $da/dN$  corresponding crack at these points. For varying the value of  $\Delta K$ , the length of the initial crack is changed between each simulation Fig. 12.

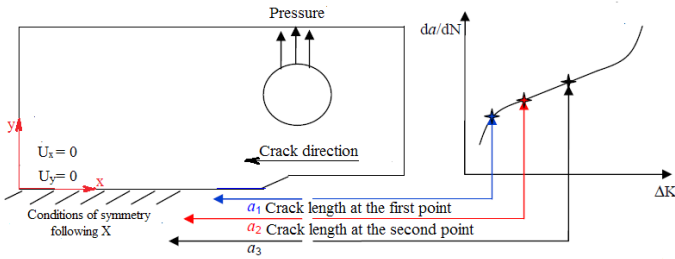


Fig. 12 Obtaining of the  $da/dN$  -  $\Delta K$  curve with the point by point method.

The relationship between  $a$ , and  $\Delta K$  is given by (2) and (3) for a given loading  $F_{amp}$ :

$$K = \frac{F \left( 2 + \frac{a}{W} \right)}{BW^{1/2} \left( 1 - \frac{a}{W} \right)^{3/2}} f \left( \frac{a}{W} \right) \quad (2)$$

$$f \left( \frac{a}{w} \right) = 0.886 + 4.64 \frac{a}{w} - 13.32 \frac{a^2}{w^2} + 14.72 \left( \frac{a}{w} \right)^3 - 5.6 \left( \frac{a}{w} \right)^4 \quad (3)$$

$F$ : is the applied load [N].

$W$ : is the width of the specimen from the loading axis [m].

$B$ : is the thickness of the test specimen [m] and  $a$ , is the crack length.

For  $0.2 < \frac{a}{w} < 0.3$  function,  $f \left( \frac{a}{w} \right)$  established by Neuman [12] is of the form:

The propagation velocities of Crack in a 6082-T6 alloy in the different areas of the same weld (Nugget, TMAZ and HAZ) for a load ratio  $R = 0.1$  for a specimen C (T). From the curves  $da/dN = \Delta K$  (Fig. 13), several outcomes can be identified.

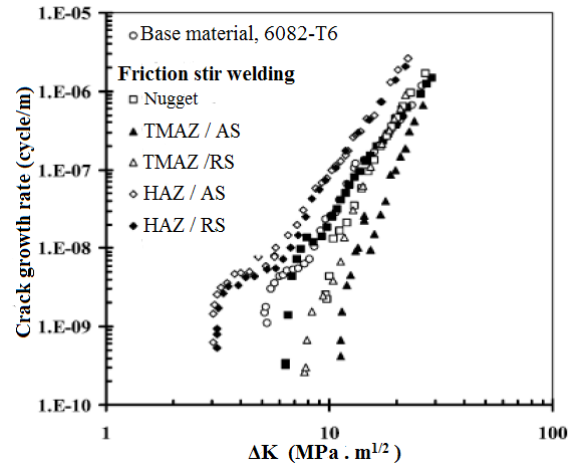


Fig. 13 Crack length according to number of cycles.

Studies report that the introduction of a plastic strain of 2% parallel to the joint makes the propagation speed of the same level as that of the base metal [23]. The resulting residual stresses than 2% plastic deformation did not affect hardness. Thus, the velocity of propagation will be primarily related to the distribution of residual stresses.

The rate of propagation of fatigue cracks depends on the ratio  $R$  (minimum / maximum stress). The presence of residual stresses in the bead welded changes the ratio [24] report that, in the longitudinal direction, the residual stresses are in tension. They are of +75 MPa in the nugget and +100 MPa in the HAZ. In the transverse direction, the residual stresses are also in tension. They are of +30 MPa in the nucleus and +40 MPa in the HAZ. The crack propagation fatigue tests performed by [10] show that the rate of spread in the nugget, the HAZ and base

metal for AA2024-T351 vary more in the longitudinal direction than in the direction cross. In addition, they report that the longitudinal fatigue crack growth threshold in the HAZ is about  $10 \text{ MPa m}^{1/2}$ , compared to  $5 \text{ MPa m}^{1/2}$  in the base metal.

## 5 Residual stresses

Residual stresses are one characteristic of welding processes. They are caused primarily by the thermal welding cycle (local heating and rapid cooling). The level of residual stress is influenced by the welding parameters. [25] report that they increase with increasing feed rate. [24] show that the change of the feed ratio changes the shape of the distribution and the maximum value of residual stresses in the longitudinal and transverse directions.

The residual stresses have compressive character by approaching the weld line, changing to a tensile character in the weld zone from the heat affected one. It can be observed that the higher values of residual stresses are achieved in the advancing side of the tool. The residual stresses values differences depend on the asymmetry of the FSW process; it is demonstrated by several finite element calculations that the higher deformation across the weld line are achieved in the retreating side of the tool when a clockwise direction is employed for the rotation.

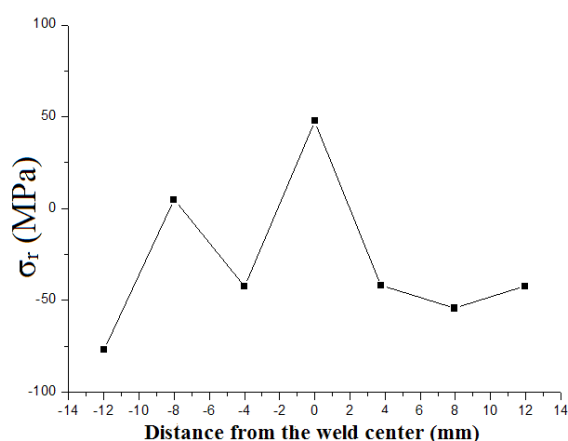


Fig. 14 Residual stress profile in longitudinal direction respect to the welding one for the fatigue tested joints.

The microstructure, hardness and residual stress distributions in the FSW are all complex. The studies in this work show each of them in three regions. These are the nugget region, the thermo mechanically affected zone and the HAZ. Each region has qualitatively or quantitatively distinct values of microstructure, hardness and residual stresses.

The nugget region has a fine recrystallised grain structure, with hardness values between 110 and 140 Hv1. within the nugget, residual stresses are low (8 MPa) parallel to the weld but large and tensile (174 MPa) perpendicular to the weld. Immediately outside the nugget, the thermo-mechanically affected zone consists of highly elongated and deformed grains, which comprise the softest (102 Hv1) part of the HAZ.

This is the region with the highest recorded residual stress in the longitudinal direction of 264 MPa, and only 5 MPa in the transverse direction. Beyond 10–12 mm the structure is only heat affected and contains a parent plate grain structure. The hardness climbs rapidly throughout the thermo-mechanically affected zone reaching a maximum at about 20–25 mm from the PJL of almost 150 Hv1. Residual stresses in this region are compressive in both longitudinal and transverse directions, the transverse component being large (192 MPa) and the longitudinal component small (13 MPa).

## 6 Conclusion

The principle of FSW welding implies that the material at the interface of the plates to be assembled is kneaded. For this, it is necessary that the material be heated to a sufficient temperature, approximately 80% of its melting temperature to facilitate mixing. Very complex process FSW where the thermal, mechanical and metallurgy remain coupled. The Purely analytical models have been developed as well as models based on methods without mesh, however, the finite element method is still the most widely used for modeling the FSW process.

The first step of this study allowed us to understand the mechanisms of FSW welding and determine in a first unlike the microstructure of welding these areas microhardness tests are used to confirm interpretations made on the heterogeneity of the structure of the solder joints.

The FSW process generates three distinct microstructural zones:

- The nugget zone (NZ)
- The thermomechanically-affected zone (TMAZ)
- The heat-affected zone (HAZ).

The HAZ is only affected by heat, without plastic deformation. The TMAZ adjacent to the nugget is plastically deformed and heated. The nugget is affected by the highest temperature and the highest plastic deformation, which generally consists of fine equiaxed grains due to the full dynamic recrystallization.

The microstructural changes are induced by the plastic deformation and the frictional heat during FSW process. A relationship between microstructure and microhardness of each FSW weld zone has been discovered. Changes in microhardness along the FSW joint are directly related to the precipitation state.

The microhardness falls dramatically in the region that is passed over by the shoulder and the microhardness reaches its lowest value in the softening region. The microhardness of TMAZ is lower than that of nugget but higher than that of HAZ. Compared with HAZ, the increase of microhardness in TMAZ can be explained by the high density of dislocations which were induced by the plastic deformation during welding. The minimum hardness is located at the interface between the TMAZ and HAZ.

The second step this study focused on the analysis of mechanical properties of the joint and the base metal.

Given the heterogeneity of FSW welding and especially that of the Nugget, it is necessary to know the areas likely to initiate the break during the various mechanical stresses (tensile and fatigue).

For a welding defect-free and properly polished, the crack propagation mechanism is related to three main elements: the residual stress, the crack initiation and the microstructure of the weld area.

This portion showed a decrease in the mechanical properties of the joint relative to the base metal.

The fatigue resistance under static and a FSW weld decreases linearly as a function of the maximum residual stress in certain conditions. The propagation velocity difference was attributed to the difference in microstructure around and in the weld zone rather than the existence of residual stresses.

Despite the fact that the residual stresses are minimal in FSW welds compared to welding of liquid phase processes, a significant quantity of these constraints may be observed, resulting in a critical deterioration of the seal and its performance in service.

## References

- [1] Thomas, W. M., Nicholas, E. D., Needham, J. C., Murch, M. G., Temple-Smith P., Dawes, C. J. "Friction-stir butt weldin." G.B. Patent No. 9125978.8, International Application No. PCT/GB92/02203. 1991.
- [2] Ericsson, M., Sandstrom, R. "Influence of welding speed on the fatigue of friction stir welds and comparison with MIG and TIG." *International Journal of Fatigue*. 25(12), pp. 1379–1387. 2003. [https://doi.org/10.1016/S0142-1123\(03\)00059-8](https://doi.org/10.1016/S0142-1123(03)00059-8)
- [3] Thomas, W. M., Nicholas, E. D. "Friction stir welding for the transportation industries." *Materials & Design*. 18(4-6), pp. 269-273. [https://doi.org/10.1016/S0261-3069\(97\)00062-9](https://doi.org/10.1016/S0261-3069(97)00062-9)
- [4] Moreira, P. M. G. P., de Figueiredo, M. A. V., de Castro, P. M. S. T. "Fatigue behaviour of FSW and MIG weldments for two aluminium alloys." *Theoretical and Applied Fracture Mechanics*. 48(2), pp. 169–177. 2007. <https://doi.org/10.1016/j.tafmec.2007.06.001>
- [5] Moreira, P. M. G. P., de Jesus, A. M. P., Ribeiro, A. S., de Castro, P. M. S. T. "Fatigue crack growth in friction stir welds of 6082-T6 and 6061-T6 aluminium alloys: A comparison." *Theoretical and Applied Fracture Mechanics*. 50(2), pp. 81-91. 2008. <https://doi.org/10.1016/j.tafmec.2008.07.007>
- [6] Kobayashi, Y., Sakuma, M., Tanaka, Y., Matsuoka, K. "Fatigue strength of friction stir welding joints of aluminium alloy 6082 extruded shape." *Welding International*. 21(1), pp. 18–24, 2007. <https://doi.org/10.1533/wint.2007.3679>
- [7] Costa, J. D., Ferreira, J. A. M., Borrego, L. P. "Influence of spectrum loading on fatigue resistance of AA6082 friction stir welds." *International Journal of Structural Integrity*. 2(2), pp. 122–134. 2011. <https://doi.org/10.1108/17579861111135888>
- [8] Jata, K. V., Sankaran, K. K., Ruschau, J. J. "Friction-stir welding effects on microstructure and fatigue of aluminum alloy 7050-T7451." *Metalurgical and Materials Transactions A*. 31(9), pp. 2181–2192. 2000. <https://doi.org/10.1007/s11661-000-0136-9>
- [9] Wan, L., Huang, Y., Guo, W., Lv, S. X., Feng, J. "Mechanical Properties and Microstructure of 6082-T6 Aluminum Alloy Joints by Self-support Friction Stir Welding." *Journal of Materials Science & Technology*. 30(12), pp. 1243-1250. 2014. <https://doi.org/10.1016/j.jmst.2014.04.009>
- [10] Bussu, G., Irving, P. E. "The role of residual stress and heat affected zone properties on fatigue crack propagation in friction stir welded 2024-T351 aluminium joints." *International Journal of Fatigue*. 25(1), pp. 77–88. 2003. [https://doi.org/10.1016/S0142-1123\(02\)00038-5](https://doi.org/10.1016/S0142-1123(02)00038-5)
- [11] Bouchouicha, B. "Contribution à l'étude de la déchirure ductile et de la propagation des fissures en fatigue dans les joints soudés." (Contribution to the study of ductile tear and the propagation of fatigue cracks in welded joints.) PhD Thesis, Djillali Liabes University of Sidi Bel Abbes, 2007. (in French)
- [12] Genevois, C. "Genèse des microstructures lors du soudage par friction malaxage d'alliages d'aluminium de la série 2000 & 5000 et comportement mécanique résultant." (Genesis of the microstructures during friction stir welding of aluminium alloys of the serie 2000 and 5000 and resulting mechanical behavior.) PhD Thesis, Institut National Polytechnique de Grenoble, 2004. (in French)
- [13] Adamowski, J., Gambaro, C., Lertora, E., Ponte, M., Szkodo, M. "Analysis of FSW welds made of aluminium alloy AW6082-T6." *Archives of Materials Science and Engineering*. 28(8), pp. 453-460. 2007.
- [14] Souto Grela, J., Blanco Viana, E. B., Martinez, D., Piñeiro, E. "Numerical simulation in welding process: optimizing structures with sequence and inertial study." *Matériaux & Techniques*. 100(4), pp. 317–326. 2012. <https://doi.org/10.1051/mattech/2012042>
- [15] Feulvarch, E. "Modélisation numérique du soudage par friction malaxage." (Numerical modeling of friction stir welding.) PhD Thesis, Université de Saint Etienne. 2005. (in French)
- [16] Rajakumar, S., Muralidharan, C., Balasubramanian, V. "Predicting tensile strength, hardness and corrosion rate of friction stir welded AA6061-T6 aluminium alloy joints." *Materials & Design*. 32(5), pp. 2878-2890. <https://doi.org/10.1016/j.matdes.2010.12.025>
- [17] Merzoug, M. "Etude paramétrique du soudage par friction malaxage." (Parametric study of friction stir welding.) PhD Thesis, Djillali Liabes University of Sidi Bel Abbes. 2011. (in French)
- [18] Data from Mechanical Laboratory of Lille (FRANCE). Laboratoire de Mécanique. Université de Lille, FRANCE
- [19] Harris, D., Norman, A. F. "Properties of friction stir welded joints: a review of literature." In: Progress report presented at the sixth PSG Meeting, pp. 17-18, 2003.
- [20] Scialpi, A., De Filippis, L. A. C., Cavaliere, P. "Influence of shoulder geometry on microstructure and mechanical properties of friction stir welded 6082 aluminium alloy." *Materials & Design*. 28(4), pp. 1124-1129. 2007. <https://doi.org/10.1016/j.matdes.2006.01.031>
- [21] Svensson, L. E., Karlsson, L., Larsson, H., Karlsson, B., Fazzini, M., Karlsson, J. "Microstructure and mechanical properties of friction stir welded aluminium alloys with special reference to AA 5083 and AA 6082." *Science and Technology of Welding and Joining*. 5(5), pp. 285-296. 2000. <https://doi.org/10.1179/136217100101538335>
- [22] ASTM E8–04, Standard Test Methods for Tension Testing of Metallic Materials. 2004.
- [23] Di, S., Yang, X., Luan, G., Jian, B. "Comparative study on fatigue properties between AA2024-T4 friction stir welds and base materials." *Materials Science and Engineering, A*. 435-436, pp. 389–395. 2006. <https://doi.org/10.1016/j.msea.2006.07.009>
- [24] Lombard, H., Hatting, D. G., Steuwer, A., James, M. N. "Optimising FSW process parameters to minimise defects and maximise fatigue life in 5083-H321 aluminium alloy." *Engineering Fracture Mechanics*. 75(3-4), pp. 341–354. 2008. <https://doi.org/10.1016/j.engfracmech.2007.01.026>
- [25] Peel, M., Steuwer, A., Preuss, M., Withers, P. J. "Microstructure, mechanical properties and residual stresses as a function of welding speed in aluminium AA5083 friction stir welds." *Acta Materialia*. 51(16), pp. 4791-4801. 2003. [https://doi.org/10.1016/S1359-6454\(03\)00319-7](https://doi.org/10.1016/S1359-6454(03)00319-7)